Journal of Alloys and Compounds xxx (xxxx) xxx

Contents lists available at ScienceDirect

Journal of Alloys and Compounds

journal homepage: http://www.elsevier.com/locate/jalcom

Effects of transition elements on the site preference, elastic properties and phase stability of $L1_2$ γ'-$Co_3(Al, W)$ from first-principles calculations

Xingjun Liu [a, c, d], Yichun Wang [a], Wei-Wei Xu [b, **], Jiajia Han [a], Cuiping Wang [a, *]

[a] College of Materials and Fujian Provincial Key Laboratory of Materials Genome, Xiamen University, Xiamen, 361005, PR China
[b] School of Aerospace Engineering, Xiamen University, Xiamen, 361005, PR China
[c] State Key Laboratory of Advanced Welding and Joining, Harbin Institute of Technology, Harbin, 150001, PR China
[d] Institute of Materials Genome and Big Data, Harbin Institute of Technology, Shenzhen, 518055, PR China

ARTICLE INFO

Article history:
Received 28 June 2019
Received in revised form
11 November 2019
Accepted 25 November 2019
Available online xxx

Keywords:
Co-based superalloys
First-principles calculations
Structural stability
Elastic properties
Thermodynamic properties

ABSTRACT

We performed a systematic study of alloying effects on the site preference, elastic properties and phase stability of $L1_2$ γ'-$Co_3(Al, W)$ in terms of the first-principles calculations. Up to twenty-one transition metal elements (Sc, Ti, V, Cr, Mn, Fe, Ni, Y, Zr, Nb, Mo, Tc, Ru. Rh, Pd, Hf, Ta, Re, Os, Ir and Pt) were considered in this work. We find that Sc, Ti, V, Cr, Mn, Y, Zr, Nb, Mo, Tc, Hf, Ta, Re and Os favor to occupy the Al site, and Fe, Ni, Ru. Rh, Pd, Ir and Pt favor to occupy the Co site, except for Y, Fe and Ru, other transition metal elements can stabilize the $L1_2$ γ'-$Co_3(Al, W)$ at 0 K. By using stress-strain method, the elastic properties including bulk modulus, shear modulus and Young's modulus were evaluated. It is verified that the elastic properties of $L1_2$ γ'-$Co_3(Al, W)$ depend on not only volume change but also electron density as well as electronic configurations. The thermodynamic results of phase stability of $L1_2$ γ'-$Co_3(Al, W)$ reveal that Hf, Ti and Ta are the promising alloying elements to improve the stability of $L1_2$ γ'-$Co_3(Al, W)$.

1. Introduction

The demands for higher-temperature capabilities motivate the continuous development of advanced superalloys for aircraft engine. The γ'-strengthened Co–Al–W-base alloys have attracted extensive interests [1] because they are less prone to freckling formation [2] and possess higher melting temperatures than Ni-based superalloys [3,4]. However, the metastability of γ'-$Co_3(Al, W)$ limits the further development of Co–Al–W superalloys in the practical application [5]. In order to alter the situation, numerous of experiments had been carried out to exploring the effects of various alloying elements on the γ'-$Co_3(Al, W)$. For instance, it is found that Ta, followed by Ti, Nb, W and Hf effectively increase the solvus temperature of γ'-$Co_3(Al, W)$ [4,6–10]. Cr, Mn and Fe tend to distribute to γ matrix and simultaneously decrease the volume fraction of the γ' precipitate [7,8]. Despite all that, the in-depth understanding of alloying effects on the site occupation, strengthening mechanism of γ'-$Co_3(Al, W)$ is quite finite, especially in experiments. Theoretically, Chen et al. [11,12] studied the site preference of transition-metal (TM) elements in the γ'-$Co_3(Al, W)$. But the results appear to conflict with the recent atom probe tomography (APT) observation [13–15], which may due to the ordered superalloys model adopted previously [11,12]. The special quasi-random structures (SQSs) model is believed to be more suitable for studying the partially disordered γ'-$Co_3(Al, W)$ [16,17]. By using the SQSs model, Xu et al. [18] investigated the effects of Ta on the electronic structure and mechanical properties of γ'-$Co_3(Al, W)$ phase, showing a well agreement between the calculated and the experimental results.

In the present study, to explore the effect of alloying elements on the properties of γ'-$Co_3(Al, W)$, the following elements are considered, *viz.*, Sc, Ti, V, Cr, Mn, Fe, Ni, Y, Zr, Nb, Mo, Tc, Ru. Rh, Pd, Hf, Ta, Re, Os, Ir and Pt. The site preference of TM in the $Co_3(Al, W)$ is firstly investigated to determine the structural configuration of TM-substituted $Co_3(Al, W)$. Secondly the elastic properties and phase stability of these TM-substituted structures are calculated. Last but

* Corresponding author.
** Corresponding author.
E-mail addresses: wwxu306@xmu.edu.cn (W.-W. Xu), wangcp@xmu.edu.cn (C. Wang).

https://doi.org/10.1016/j.jallcom.2019.153179
0925-8388/

not least, the bonding characteristic is analyzed to gain an insight into affecting mechanism of TM in the $Co_3(Al, W)$ phase. The present work provides a theoretical foundation for further development of novel γ/γ′ Co-based superalloys.

2. Computational methods and details

2.1. Reaction and stable formation energies

The $L1_2$-type γ′-$Co_3(Al, W)$ shows a formula A_3B with space group Pm-3m. The A atoms are located at the face centers, and the B atom is located at the cube corner. In order to compare the experimental composition (Co−10Al−11W (at.%) [1]), a SQSs supercell with 32 atoms constructed by Jiang et al. [16] was adopted in present study, as shown in Fig. 1. Only one TM atom was selected for doping in the structure to obtain a comparable TM component with the experiment. In the structure of $Co_3(Al, W)$ as shown in Fig. 1, there are seven nonequivalent positions (Al_1/Al_2, $Co_3/Co_4/Co_5$ and W_6/W_7) for the substitution by TM.

The reaction energy (E_d^i) is introduced to study the alloying effect on the site preference in the $Co_3(Al, W)$, which is defined as the energy difference between $Co_3(Al, W)$ with one of nonequivalent positions (i) substituted by TM and TM-free $Co_3(Al, W)$ by Ref. [19]:

$$E_d^i = \left[E_t^D(Co_3(Al,W)) + \mu_i\right] - \left[E_t^P(Co_3(Al,W)) + \mu_{TM}\right] \quad (1)$$

where E_t^D is the static energy of TM-substituted $Co_3(Al, W)$, E_t^P is the static energy of TM-free $Co_3(Al, W)$, μ_i and μ_{TM} are the chemical potential of Co, Al, W and TM atoms. Under Co-rich conditions, μ_{Co} is assumed to be the static energy of Co [19], whereas μ_{Al} and μ_W are calculated by the following relationships [18]:

$$\begin{cases} \mu_{Co} + \mu_{Al} = E_t^P(CoAl) \\ 3\mu_{Co} + \mu_W = E_t^P(Co_3W) \end{cases} \quad (2)$$

Taking the case of TM doping Al_1 position as example, the negative E_d^{Al1} means that the energy of the right side of the equation (*i.e.*, $Co_{24}Al_4W_4 + TM \rightarrow Co_{24}Al_3W_4TM + Al$) is lower than that of the left side, indicating the possibility of TM doping Al_1 position. On the other hand, if the reaction energy for the Al_1-doped case is lower than those for other i-doped cases, it implies that the TM tends to occupy Al_1 positions.

As long as the site preferences of alloying elements in $L1_2$ $Co_3(Al, W)$ were determined, the relative phase stability could then be evaluated by the stable formation energy (ΔH_s^{TM}), which is defined with respect to the convex hull consisting of set of potential stable binary and unary structures (*i.e.*, hcp-Co + B2−CoAl + $D0_{19}$-Co_3W + TM) at the fixed composition. It is noteworthy that the pure TM instead of Co_3TM is chose to constitute the convex hull due to the sufficient dilute concentration of TM and the uncertain existence of Co_3TM. Taking the case of TM doping Al_1 position as example, $\Delta H_s^{TM}(Al_1)$ is written as [20]:

$$\Delta H_s^{TM}(Al_1) = E_t^D\left(Co_3\left(Al_{3/8}W_{4/8}TM_{1/8}\right)\right) - \sum_i \mu_{mix} \quad (3)$$

$$\sum_i \mu_{mix} = 9\Big/32E_t^P(Co) + 3\Big/32E_t^P(CoAl) + 4\Big/32E_t^P(Co_3W) + 1\Big/32E_t^P(TM) \quad (4)$$

If the stable formation energy is positive, $\Delta H_s^{TM} > 0$, it means that TM-substituted $Co_3(Al, W)$ phase is difficult to be formed, compared with the four-phase mixture (hcp-Co, B2−CoAl, D019-Co3W, pure-TM). When $\Delta H_s^{TM} < 0$, it means that TM-substituted $Co_3(Al, W)$ phase likely to be formed, in addition, a more negative ΔH_s^{TM} of a crystal phase indicate that the crystal is more stable.

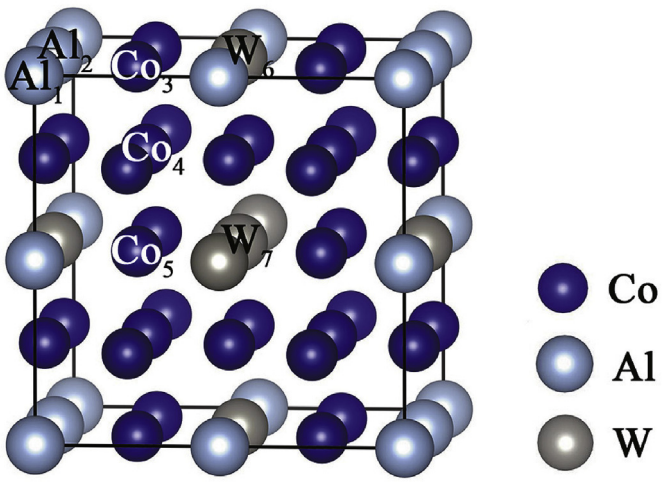

Fig. 1. Crystal structure of $L1_2$-ordered $Co_3(Al, W)$. There are seven nonequivalent positions (Al_1/Al_2, $Co_3/Co_4/Co_5$ and W_6/W_7) for the substitution by TM.

2.2. Elastic properties

The elastic constants (C_{ij}) are calculated using the stress-strain method [21]. The cell shape and volume are fixed during the relaxations of ionic positions, and only the forces acting on ions can be relaxed. Based on the Hooke's law, the elastic stiffness constants are defined as:

$$\sigma_i = \sum_j C_{ij} \cdot \varepsilon_i = \begin{pmatrix} \sigma_1 \\ \sigma_2 \\ \sigma_3 \\ \sigma_4 \\ \sigma_5 \\ \sigma_6 \end{pmatrix} = \begin{pmatrix} C_{11} & C_{12} & C_{13} & C_{14} & C_{15} & C_{16} \\ C_{21} & C_{22} & C_{23} & C_{24} & C_{25} & C_{26} \\ C_{31} & C_{32} & C_{33} & C_{34} & C_{35} & C_{36} \\ C_{41} & C_{42} & C_{43} & C_{44} & C_{45} & C_{46} \\ C_{51} & C_{52} & C_{53} & C_{54} & C_{55} & C_{56} \\ C_{61} & C_{62} & C_{63} & C_{64} & C_{65} & C_{66} \end{pmatrix} \times \begin{pmatrix} \varepsilon_1 \\ \varepsilon_2 \\ \varepsilon_3 \\ \varepsilon_4 \\ \varepsilon_5 \\ \varepsilon_6 \end{pmatrix} \quad (5)$$

where σ_i and ε_i represent the stress vector and the strain vector,

Please cite this article as: X. Liu et al., Effects of transition elements on the site preference, elastic properties and phase stability of $L1_2$ γ′-$Co_3(Al, W)$ from first-principles calculations, Journal of Alloys and Compounds, https://doi.org/10.1016/j.jallcom.2019.153179

respectively. For a given set of strains, $\varepsilon = (\varepsilon_1, \varepsilon_2, \varepsilon_3, \varepsilon_4, \varepsilon_5, \varepsilon_6)$ where $\varepsilon_1, \varepsilon_2, \varepsilon_3$ refer to normal strains and $\varepsilon_4, \varepsilon_5, \varepsilon_6$ refer to shear strains, are imposed on a crystal to generate the small deformations. One set of stress $\sigma = (\sigma_1, \sigma_2, \sigma_3, \sigma_4, \sigma_5, \sigma_6)$ can be determined on the deformed lattice from first principles calculation. Due to the crystal symmetry, the independent elastic constant matrix $\boldsymbol{C}$ for $L1_2$-type structure were calculated according to the following equation:

$$\boldsymbol{C} = \varepsilon^{-1} \cdot \sigma \cdot \begin{pmatrix} C_{11} & C_{12} & C_{13} & 0 & 0 & 0 \\ C_{21} & C_{22} & C_{23} & 0 & 0 & 0 \\ C_{31} & C_{32} & C_{33} & 0 & 0 & 0 \\ 0 & 0 & 0 & C_{44} & 0 & 0 \\ 0 & 0 & 0 & 0 & C_{55} & 0 \\ 0 & 0 & 0 & 0 & 0 & C_{66} \end{pmatrix} \quad (6)$$

where $\boldsymbol{C}$ is an 6×6 elastic stiffness constant matrix with C_{ij}, and ε^{-1} represents the (pseudo) inverse of the sets of strains. More details are described in Ref. [22]. After the substitution of TM, the cubic lattice of Co_3(Al, W) may be slightly distorted, resulting in the increase of independent C_{ij}. To ensure the comparability of our calculated results, average C_{ij} were used here as:

$$\overline{C}_{11} = (C_{11} + C_{22} + C_{33})/3, \quad \overline{S}_{11} = (S_{11} + S_{22} + S_{33})/3 \quad (7)$$

$$\overline{C}_{12} = (C_{12} + C_{13} + C_{23})/3, \quad \overline{S}_{12} = (S_{12} + S_{13} + S_{23})/3 \quad (8)$$

$$\overline{C}_{44} = (C_{44} + C_{55} + C_{66})/3, \quad \overline{S}_{44} = (S_{44} + S_{55} + S_{66})/3 \quad (9)$$

where S_{ij} are elastic compliance constants obtained from the inverse of C_{ij} matrix. The aggregate properties of polycrystals (*i.e.*, bulk (B), shear (G), Young's (E) moduli and Poisson's ratio (ν)) can calculated by Refs. [23–25]:

$$B_V = (\overline{C}_{11} + 2\overline{C}_{12})/3, \quad B_R = 1/(3\overline{S}_{11} + 6\overline{S}_{12}) \quad (10)$$

$$G_V = (\overline{C}_{11} - \overline{C}_{12} + 3\overline{C}_{44})/5, \quad G_R = 5/(4\overline{S}_{11} - 4\overline{S}_{12} + 3) \quad (11)$$

$$B_H = (B_V + B_R)/2 \quad (12)$$

$$G_H = (G_V + G_R)/2 \quad (13)$$

$$E_H = (9B_H G_H)/(3B_H + G_H) \quad (14)$$

$$\nu = 3B_H - 2G_H/2(3B_H + G_H) \quad (15)$$

2.3. Details of first-principles calculations

All calculations were performed by the projector augmented wave (PAW) method [26], which is implemented in the Vienna *Ab initial* Simulation Package (VASP) [27,28]. The Perdue-Burke-Ernzerhof (PBE) [29] was used to describe the exchange and correlation functional. The standard valence shells and electronic configurations were used for all the mentioned elements. A 450 eV kinetic energy cutoff of wave function was used. The Brillouin zone sampling was performed with a Γ-centered $7 \times 7 \times 7$ k-point mesh. Reciprocal space integration was performed by means of the Methfessel-Paxton technique [29] with a smearing width of 0.15 eV. Throughout the calculations, the convergence thresholds of total energy and the maximum force acting on ions were set to 10^{-4} eV/atom and 10^{-2} eV/Å, respectively. The spin polarization was considered because of the ferromagnetic nature of Co.

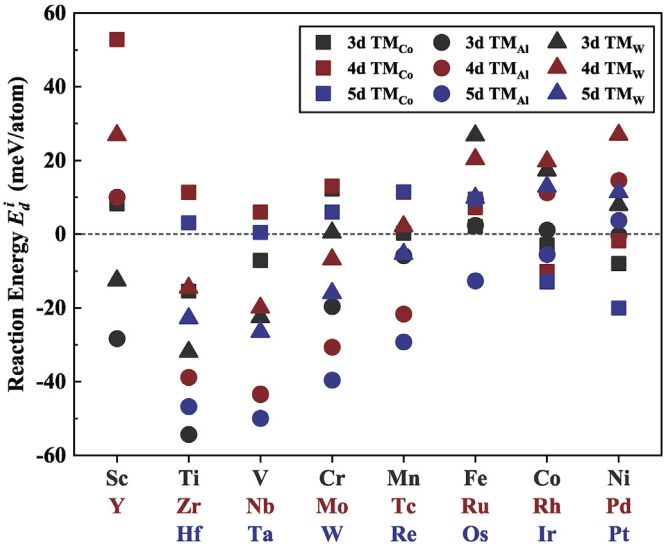

Fig. 2. The calculated reaction energy for the Co_3(Al, W) doped with 3d-, 4d- and 5d-TM elements. (square, round and triangle mean that TM occupies the sites of Co, Al and W, respectively.)

3. Results and discussion

3.1. Site preference and structural stability

Fig. 2 plots the calculated reaction energy E_d^i for the Co_3(Al, W) doped with 3d-, 4d- and 5d-TM to evaluate the relative site preference. Note that only the minimum reaction energy for the TM doping the different nonequivalent positions of Co_3(Al, W) was shown in Fig. 2. As seen, the TM elements locating at the left side of periodic table (*i.e.*, IVa and Va subgroup) show lower E_d^i values than those at the right side of periodic table (*i.e.*, VIII subgroup). By comparing the E_d^i values, it is concluded that Sc, Ti, V, Cr, Mn, Y, Zr, Nb, Mo, Tc, Hf, Ta, Re and Os prefer to occupy the Al site, and Fe, Ni, Ru, Rh, Pd, Ir and Pt prefer to occupy the Co site. The W site is energetically unfavorable for occupation since it shows a maximum E_d^i after TM doping. Our results reproduce the experimental observations by atom probe tomography and channeling enhanced microanalysis [13,15,30–32] that Ti, V, Mo, Ta, Cr favors the Al/W site, and Ni favors the Co site. The agreement indicates the reliable of the present work. After confirming the lowest-energy structure for TM-substituted Co_3(Al, W), their structural properties including equilibrium volume (V_{eq}), total energy (E_{tot}) were calculated and are tabulated in Table 1. The predicted V_{eq} and E_{tot} of Co_3(Al, W) well agree the previous theoretical and experimental results [1,18,33] with an average deviation less than 3%.

To estimate the relative phase stability of TM-substituted Co_3(Al, W) listed in Table 1, the stable formation energy (ΔH_s^{TM}) was calculated based on Eqs. (3) and (4). The result is shown in Fig. 3. A negative value of ΔH_s^{TM} indicates that the phase can be steadily synthesized. More negative ΔH_s^{TM}, more stable the phase exists. As seen from Fig. 3, all the TM-substituted structures own positive ΔH_s^{TM} values, suggesting they are metastable at 0 K. Despite all that, comparing to the TM-free Co_3(Al, W) (67.48 meV/atom), the addition of TM except Y, Fe and Ru significantly decreases the ΔH_s^{TM}. It implies that these TM elements improve the stability of Co_3(Al, W), especially Ti, Ta, Hf, Nb, V and Zr. It is worth noting that Y, Fe and Ru will be abandoned in the subsequent studies since they are unbeneficial to enhance the phase stability of Co_3(Al, W).

Please cite this article as: X. Liu et al., Effects of transition elements on the site preference, elastic properties and phase stability of $L1_2$ γ'-Co_3(Al, W) from first-principles calculations, Journal of Alloys and Compounds, https://doi.org/10.1016/j.jallcom.2019.153179

Table 1
Calculated and experimental equilibrium volumes (V_{eq}), total energies (E_{tot}), reaction energy (E_d^i) and stable formation energy (ΔH_s^{TM}) of TM-substituted $Co_3(Al, W)$, which TM occupies the minimum E_d^i value site. (V_{eq}, E_{tot} are given in eV/atom, while E_d^i, ΔH_s^{TM} are given in meV/atom).

Compound	Designation	site	V_{eq}	E_{tot}	E_d^i	ΔH_s^{TM}
$Co_{24}(Al_4W_4)$	Pure		11.320	−7.491		67.475
			11.337[a]	−7.476[a]		44.871[a]
			11.327[b]			
			11.654[c]			
$Co_{24}(Al_3W_4Sc)$	Sc_{Al}	Al_2	11.531	−7.560	−19.647	47.366
$Co_{24}(Al_3W_4Ti)$	Ti_{Al}	Al_2	11.360	−7.635	−46.577	20.433
$Co_{24}(Al_3W_4V)$	V_{Al}	Al_2	11.286	−7.661	−35.474	31.536
$Co_{24}(Al_3W_4Cr)$	Cr_{Al}	Al_2	11.246	−7.657	−12.611	54.399
$Co_{24}(Al_3W_4Mn)$	Mn_{Al}	Al_2	11.249	−7.623	−3.563	63.447
$Co_{23}Fe(Al_4W_4)$	Fe_{Co}	Co_3	11.404	−7.527	**4.276**	**71.283**
$Co_{23}Ni(Al_4W_4)$	Ni_{Co}	Co_3	11.402	−7.450	**−5.334**	**61.676**
$Co_{24}(Al_3W_4Y)$	Y_{Al}	Al_2	11.654	−7.527	20.070	87.080
$Co_{24}(Al_3W_4Zr)$	Zr_{Al}	Al_2	11.527	−7.642	−28.558	38.452
$Co_{24}(Al_3W_4Nb)$	Nb_{Al}	Al_2	11.426	−7.700	−33.171	33.839
$Co_{24}(Al_3W_4Mo)$	Mo_{Al}	Al_2	11.368	−7.708	−21.201	45.809
$Co_{24}(Al_3W_4Tc)$	Tc_{Al}	Al_2	11.336	−7.681	−11.516	55.494
$Co_{23}Ru(Al_4W_4)$	Ru_{Co}	Co_3	11.455	−7.553	**8.594**	**75.604**
$Co_{23}Rh(Al_4W_4)$	Rh_{Co}	Co_3	11.508	−7.508	**−5.646**	**61.364**
$Co_{23}Pd(Al_4W_4)$	Pd_{Co}	Co_3	11.478	−7.436	**6.172**	**73.182**
$Co_{24}(Al_3W_4Hf)$	Hf_{Al}	Al_2	11.511	−7.693	−38.260	28.750
$Co_{24}(Al_3W_4Ta)$	Ta_{Al}	Al_2	11.431	−7.756	−41.284	25.726
$Co_{24}(Al_3W_4Re)$	Re_{Al}	Al_2	11.349	−7.754	−19.539	47.471
$Co_{24}(Al_3W_4Os)$	Os_{Al}	Al_2	11.344	−7.701	−4.119	62.891
$Co_{23}Ir(Al_4W_4)$	Ir_{Co}	Co_3	11.504	−7.561	**−10.352**	**56.658**
$Co_{23}Pt(Al_4W_4)$	Pt_{Co}	Co_3	11.552	−7.482	**−13.505**	**53.505**

[a] Calculation data [18].
[b] Experimental data [33].
[c] Experimental data [1].

3.2. Alloying effects on mechanical properties

In order to explore alloying effects on the mechanical properties, the elastic properties of TM-substituted $Co_3(Al, W)$ were calculated, including elastic constants ($\overline{C}_{ij}$), bulk modulus (B), shear modulus (G), Young's modulus (E), Poisson's ratio (ν). The results are listed in Table 2, as well as the available theoretical and experimental data [18,34] for comparison. A good agreement is found for our calculated results and those from the previous studies [18,34]. Although the elastic constants are remarkably changed by the addition of TM, it is shown that all of the $L1_2$ TM-substituted $Co_3(Al, W)$ are mechanically stable, since their C_{ij} values meet the Born criteria [35] which is represented by:

$$C_{11} > 0, C_{44} > 0, C_{11} > |C_{12}|, (C_{11} + 2C_{12}) > 0 \quad (16)$$

In an effort to seek the effect trend of TM on the elastic properties of $Co_3(Al, W)$, Fig. 4 plots the elastic properties as a function of volume changes for TM-substituted $Co_3(Al, W)$. It is indicated that the doped structure with small volume change will result in a large change in bulk and shear moduli. The addition of alloying elements preferred to occupy Co sites increases the volume of $Co_3(Al, W)$ while the addition of those preferred to occupy Al sites does opposite. This phenomenon can be explained by the effect of the relative metallic atomic radii of TM as compared to Co/Al atom. Generally, these metallic atoms (Ni, Rh, Pd, Ir and Pt) have larger radii than Co but smaller than Al. Therefore, the volumes of compounds expand when the alloying elements occupy Co sites but shrink when the alloying elements occupy Al sites.

For all the TM occupying Co sites, it is found that both B and G increase almost linearly with the volume change as shown in Fig. 4(a)–(b). But for the TM occupying Al sites, the 3d and 5d TM decrease these moduli of $Co_3(Al, W)$ with the increase of the volume, while the 4d TM shows an opposite influence. This suggests that the volume change could not be the exclusive effect on the elastic properties. According to an empirical relationship related to the bulk modulus (B) per molar volume (V_m) and electron density, $\sqrt{B/V_m}$ has a linear relationship with the electron density [36,37]. This suggests that the electron density may be the other one key factor, which can be calculated via $n = Z_B/V_m$, where Z_B is the bond valence. The total number of valence electrons N contained in $A_{1-x-y}B_xC_y$ is calculated by $N = (1-x-y)n_AV_A + xn_BV_B + yn_CV_C$ where n_A, n_B and n_C are the electron density, and V_A, V_B and V_C are the molar volume of element A, B and C, respectively. For the $L1_2$ TM-substituted $Co_3(Al, W)$, the electron density n can be deduced by:

$$n_{TM_{Co}} = N \Big/ V = \left(\frac{23}{32}n_{Co}V_{Co} + \frac{4}{32}n_{Al}V_{Al} + \frac{4}{32}n_WV_W + \frac{1}{32}n_{TM}V_{TM}\right) \times \Big/ V_{TM_{Co}} \quad (17)$$

$$n_{TM_{Al}} = N \Big/ V = \left(\frac{24}{32}n_{Co}V_{Co} + \frac{3}{32}n_{Al}V_{Al} + \frac{4}{32}n_WV_W + \frac{1}{32}n_{TM}V_{TM}\right) \times \Big/ V_{TM_{Al}} \quad (18)$$

$$n_{TM_W} = N \Big/ V = \left(\frac{24}{32}n_{Co}V_{Co} + \frac{4}{32}n_{Al}V_{Al} + \frac{3}{32}n_WV_W + \frac{1}{32}n_{TM}V_{TM}\right) \times \Big/ V_{TM_W} \quad (19)$$

where the electron densities (n_{Co}, n_{Al}, n_W and n_{TM}) are calculated from equilibrium volume and valence of pure elements [38]. Fig. 4(c) illustrates the n dependence of $\sqrt{B/V_m}$ for the TM-substituted-$Co_3(Al, W)$. To facilitate visualization, the values were linearly fitted respectively for elements of each period, in which the arrow represents the direction of volume reduction according to

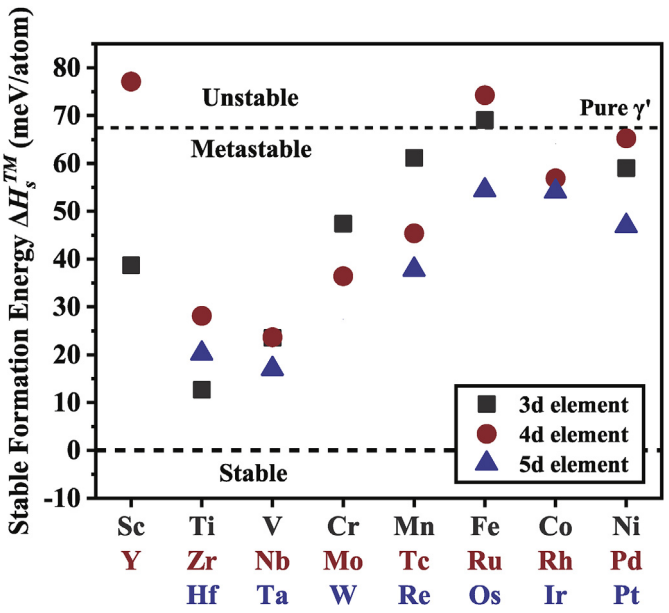

Fig. 3. The calculated stable formation energy of TM-substituted $Co_3(Al, W)$.

Table 2
Calculated elastic constants C_{ij}, bulk modulus B, shearing modulus G, Young's modulus E, B/G, Poisson's ratio ν and universal anisotropy index A^U of $L1_2$ TM-substituted $Co_3(Al, W)$.

Compound	Designation	$\overline{C}_{11}$	$\overline{C}_{12}$	$\overline{C}_{44}$	B	G	E	B/G	ν	A^U
$Co_{24}(Al_4W_4)$	Pure	304	181	177	222	116	296	1.92	0.278	1.48
		284[a]	163[a]	174[a]	203[a]	114[a]	288[a]	1.78[a]	0.260[a]	
		271[b]	172[b]	162[b]	205[b]	101[b]	260[b]	2.03[b]	0.290[b]	
$Co_{24}(Al_3W_4Sc)$	Sc_{Al}	323	182	176	229	122	311	1.88	0.274	1.08
$Co_{24}(Al_3W_4Ti)$	Ti_{Al}	336	190	183	239	126	323	1.89	0.275	1.11
$Co_{24}(Al_3W_4V)$	V_{Al}	360	184	188	243	139	349	1.75	0.260	0.72
$Co_{24}(Al_3W_4Cr)$	Cr_{Al}	373	182	192	245	145	364	1.69	0.253	0.61
$Co_{24}(Al_3W_4Mn)$	Mn_{Al}	358	175	182	234	138	345	1.70	0.254	0.69
$Co_{23}Ni(Al_4W_4)$	Ni_{Co}	294	174	171	214	113	287	1.90	0.276	1.45
$Co_{24}(Al_3W_4Zr)$	Zr_{Al}	331	183	178	232	125	318	1.86	0.272	1.00
$Co_{24}(Al_3W_4Nb)$	Nb_{Al}	360	183	186	242	138	348	1.76	0.261	0.69
$Co_{24}(Al_3W_4Mo)$	Mo_{Al}	372	181	186	245	142	358	1.72	0.257	0.56
$Co_{24}(Al_3W_4Tc)$	Tc_{Al}	377	179	189	245	145	364	1.69	0.252	0.52
$Co_{23}Rh(Al_4W_4)$	Rh_{Co}	305	189	176	227	113	291	2.01	0.287	1.65
$Co_{23}Pd(Al_4W_4)$	Pd_{Co}	295	181	172	219	110	283	1.99	0.284	1.63
$Co_{24}(Al_3W_4Hf)$	Hf_{Al}	333	187	178	235	124	317	1.89	0.275	1.03
$Co_{24}(Al_3W_4Ta)$	Ta_{Al}	369	190	187	250	139	352	1.80	0.265	0.68
		352[a]	187[a]	181[a]	242[a]	132[a]	335[a]	1.83[a]	0.270[a]	
$Co_{24}(Al_3W_4Re)$	Re_{Al}	383	184	192	250	147	369	1.69	0.253	0.55
$Co_{24}(Al_3W_4Os)$	Os_{Al}	378	179	189	245	146	366	1.68	0.252	0.51
$Co_{23}Ir(Al_4W_4)$	Ir_{Co}	318	197	178	237	116	299	2.05	0.290	1.56
$Co_{23}Pt(Al_4W_4)$	Pt_{Co}	307	192	177	230	113	291	2.04	0.289	1.69

[a] DFT calculation data [18].
[b] Experiment data [33].

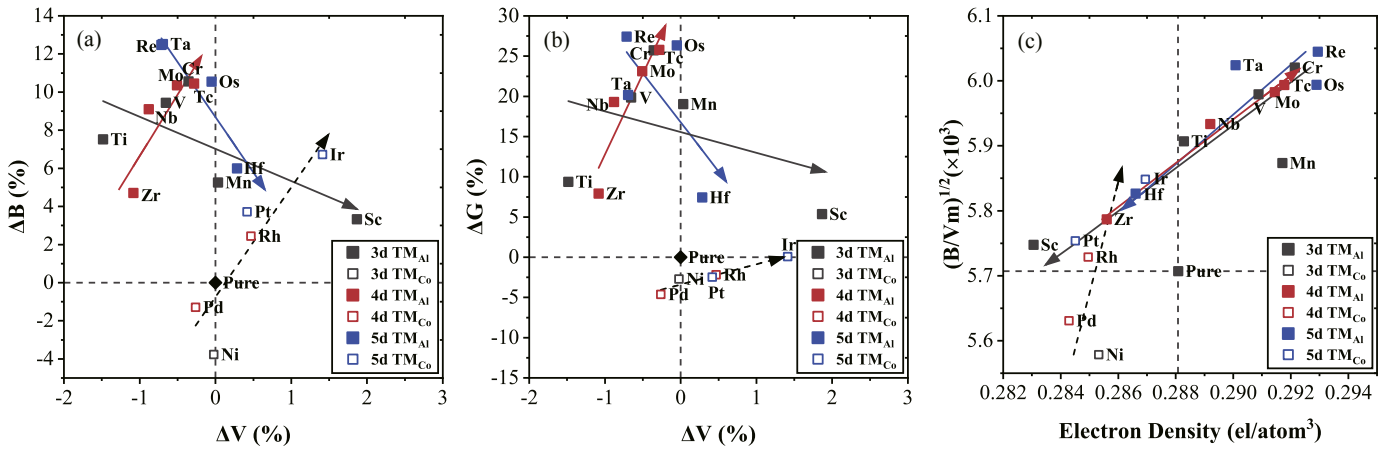

Fig. 4. The elastic properties of the $L1_2$ TM-substituted $Co_3(Al, W)$: (a) Correlation between Bulk modulus change and equilibrium volume change; (b) Correlation between Shear modulus change and equilibrium volume change; (c) Correlation between $(B/V_m)^{0.5}$ and electron density n, B in GPa, and V_m in 10^{-6} m^3/mol.

Fig. 4(a). In Fig. 4(c), the change tendency of $\sqrt{B/V_m}$ for the Co-occupied elements (black dotted line) is consistent with that for the 4d Al-occupied elements (red line), and it is also true for the case of the 3d Al-occupied elements (black line) and the 5d Al-occupied elements (blue line). The monotonically proportional relationship between electron density n and $\sqrt{B/V_m}$ explains the difference in variation observed from Fig. 4(a)–(b).

On the other hand, the B/G ratio is an indicator of brittle/ductile behavior of materials. A high B/G value indicates a tendency for ductility while a low B/G value indicates brittleness. The critical value between ductility and brittleness is considered to be 1.75 [39]. From Table 2, one can find that the addition of TM occupying Co sites increases the value of B/G compared to TM-free $Co_3(Al, W)$, meaning the increase of ductility by doping TM. In addition, the Cauchy pressure (C_{12}—C_{44}) is proposed to reflect the bonding nature [40]. A positive Cauchy pressure indicates a metallic bonding, while a negative one indicates the covalent bonding. Moreover, the larger the Cauchy pressure, the greater the toughness of materials.

To clarify the inherent correlation between ductile-brittle and bonding nature, Fig. 5 plots the B/G ratio versus (C_{12}—C_{44}) for the $L1_2$ TM-substituted $Co_3(Al, W)$. Apparently, the B/G values are linearly proportional to (C_{12}—C_{44}), indicating the ductile feature is largely contributed from the metallic bonding nature. The more the proportion of metallic bonding, the more ductile the TM-substituted $Co_3(Al, W)$ exhibit. In particular, adding TM elements preferred to occupy Co sites (*i.e.*, Rh, Pd, Ir, and Pt) is the most effective way to enhance the ductility of $Co_3(Al, W)$ as seen in Fig. 5. That is, occupying the A site of $L1_2$-type A_3B is more inclined to form the metallic bonding, while occupying the B site is more inclined to form the covalent bonding.

3.3. Electronic structure

The charge density difference (CDD) was introduced to study the bonding electrons to gain an insight into the effect of TM elements on the mechanical properties of $L1_2$-$Co_3(Al, W)$. The CDD is defined

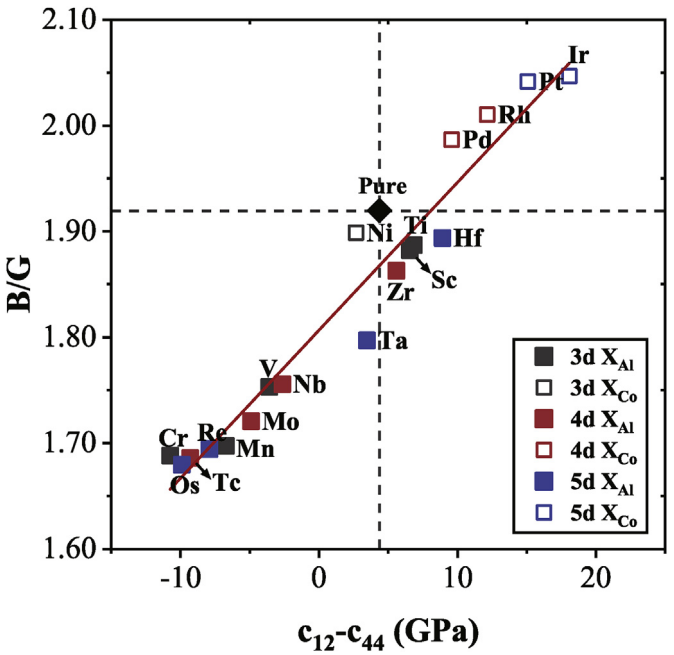

Fig. 5. Correlation between B/G and $C_{12}-C_{44}$ for the $L1_2$ TM-substituted $Co_3(Al, W)$.

as the charge density difference between self-consistent and nonself-consistent calculations. Fig. 6 illustrates the CDD in the (001) plane for four typical TM-substituted structures (*i.e.*, Re_{Al}, Sc_{Al}, Ir_{Co}, Pd_{Co}) because the Re_{Al} and the Ir_{Co} show the maximum shear moduli while the Sc_{Al} and the Pd_{Co} yield the minimum ones.

As seen from Fig. 6(a), there has a noticeable directional distribution of charge density between the Co–W and Co–Al bonds in the TM-free $Co_3(Al, W)$. It implies that the covalent-like bonding is pronounced in this spatial orientation. For Re_{Al} (Fig. 6(b)), the Co–Re bonds are distorted in shape and are stronger than the Co–Al bonds. Moreover, the angular shape of charge density is sustained. This strong covalent hybridization and the relevant angular shape of charge density enhance the stiffness of chemical bonds, leading to a remarkable increase of shear moduli. For Sc_{Al} (Fig. 6(c)), the addition of Sc decreases the quantity of transfer electrons between Co and Sc atoms, but increase the electron density between Co and Al atoms. Under this circumstance, the shear modulus of Sc_{Al} is thus lower than that of Re_{Al}. For the TM occupying Co sites (*i.e.*, Ir_{Co} and Pd_{Co}), however, the situation is rather different. For Ir_{Co} (Fig. 6(d)), the addition of Ir lead to the charge density asymmetrical distribution around the Co–W and Ir–W directions. Such asymmetrical electronic distribution weakens the covalent strengthening effect, and thus results in a lower shear modulus for Ir_{Co} than that for TM-free $Co_3(Al, W)$. For Pd_{Co} (Fig. 6(e)), the addition of Pd also lead to the charge density asymmetrical distribution, but the CDD around the Pd atom are excessively diluted, weakening the Ir–W bonds, resulting in a significant decrease in the shear modulus.

For asymmetric electronic structures, the anisotropy of supercell can be quantified by the universal anisotropy index [41]:

$$A^U = 5G^V/G^R + B^V/B^R - 6 \quad (20)$$

where G^V, G^R, B^V and B^R are calculated with Eqs. (10)–(13). The larger value of A^U, the more anisotropic. The calculated values of A^U are listed in Table 2. By associating the anisotropy index with the shear modulus for each compound, we found an inversely proportional relationship between them, a larger degree of anisotropy of CDD generally indicates a smaller shear modulus.

3.4. Phase stability at high temperatures

The mechanical properties of the Co–Al–W-based superalloy cannot be stably maintained at high temperatures. Suzuki et al. [42] considered that the straitness of phase region of γ′-$Co_3(Al, W)$ is the primary reason of this phenomenon. As the annealing time

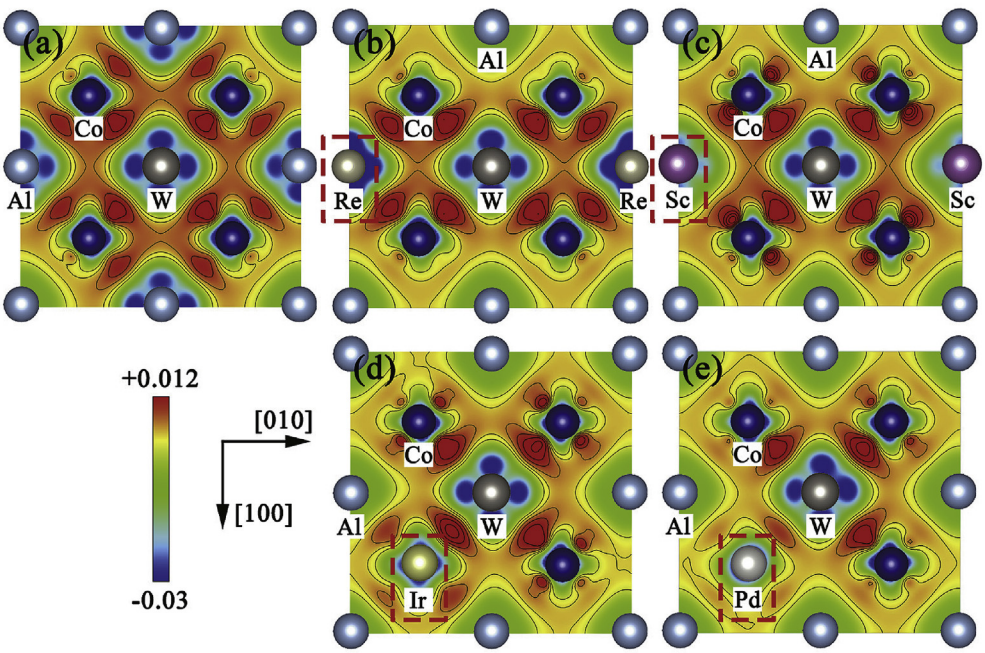

Fig. 6. The calculated charge density difference (CDD) in the (001) plane for TM-free and TM-substituted $L1_2$-$Co_3(Al, W)$; (a) TM-free; (b) Re occupying Al site; (c) Sc occupying Al site; (d) Ir occupying Co site; (e) Pd occupying Co site.

Please cite this article as: X. Liu et al., Effects of transition elements on the site preference, elastic properties and phase stability of $L1_2$ γ′-$Co_3(Al, W)$ from first-principles calculations, Journal of Alloys and Compounds, https://doi.org/10.1016/j.jallcom.2019.153179

increase, the γ′-Co_3(Al, W) phase will decomposed to $D0_{19}$ or B2 phase. The decomposed products is depended on the initial alloy composition [5]. In the current case that the proportion of W is higher than Al, γ′-Co_3(Al, W) phase is mainly decomposed into $D0_{19}$ phase. Accordingly, $D0_{19}$ phase was considered as the competitive phase against $L1_2$ phase to evaluate the phase stability at finite temperatures.

The quasi-harmonic Debye model [43] was adopted to compute the Gibbs free energies of the $L1_2$-and $D0_{19}$-type of TM-substituted Co_3(Al, W). All thermodynamic calculations were performed by Gibbs2 package [44]. The relevant data of the $D0_{19}$ TM-substituted Co_3(Al, W) is provided in the *Supplementary*. The stability of TM-substituted Co_3(Al, W) can be accessed by Gibbs free energy difference which is defined as:

$$\Delta G = G_{D0_{19}} - G_{L1_2} \tag{21}$$

where G_{L1_2} and $G_{D0_{19}}$ are the Gibbs free energies of the $L1_2$-and $D0_{19}$-type structures, respectively. If $\Delta G < 0$, then the $D0_{19}$ structure is preferred, and if $\Delta G > 0$, then the $L1_2$ structure is preferred, but it doesn't mean that $L1_2$-type TM substituted Co_3(Al, W) can be stably existed in the temperature range of $\Delta G > 0$. Fig. 7 shows the calculated ΔG values as a function of temperatures for TM-substituted Co_3(Al, W). It is obvious indicated that the ΔG values along whole temperature range of TM-free Co_3(Al, W) is negative. It implies that it is energetically favorable of $D0_{19}$ structure instead of $L1_2$ structure, and thus demonstrates the metastability of $L1_2$-Co_3(Al, W) in experiments [5]. On the other hand, the TM-substituted Co_3(Al, W) shows higher ΔG than the TM-free one. It means that the addition of TM, especially Hf, Ti, Ta, Sc, Zr, Nb and Mo, is beneficial to improve the stability of Co_3(Al, W) at finite temperatures. Our conclusion is consistent with the recent experimental observations [6–9] that these strong γ′-former elements can increase the solvus temperature of γ′ phase.

In order to estimate the structural stability at high temperatures, the volume thermal expansion coefficient α were calculated. Fig. 8 depicts the calculated α of both TM-free and TM-substituted $L1_2$-Co_3(Al, W) at finite temperatures. In general, the value of α increases sharply up to ~300 K for all the alloying Co_3(Al, W) and show a similar tendency as the increasing temperature. Distinguishingly, the value of α of Mn, Ir, Sc, Rh, Pt and Ni is much higher than other TM, which becomes more significant at high temperatures. It means that the addition of Mn, Ir, Sc, Rh, Pt and Ni would cause the remarkable expansion of γ′ phase, and further indicates these elements would not be good candidates for improving the structural stability of γ′-Co_3(Al, W).

4. Conclusions

The alloying effect of transition-metal (TM) elements on the site preference, elastic properties and phase stability of $L1_2$ γ′-Co_3(Al, W) have been studied from first-principles calculations. Twenty-one TM elements, namely, Sc, Ti, V, Cr, Mn, Fe, Ni, Y, Zr, Nb, Mo, Tc, Ru. Rh, Pd, Hf, Ta, Re, Os, Ir and Pt, have been considered. The main results are summarized as follows:

1. Sc, Ti, V, Cr, Mn, Y, Zr, Nb, Mo, Tc, Hf, Ta, Re and Os prefer to occupy the Al site, while Fe, Ni, Ru, Rh, Pd, Ir and Pt prefer to occupy the Co site. All TM-substituted structures are metastable at 0 K. Despite all that, comparing to the TM-free Co_3(Al, W), the addition of TM can improves the stability of Co_3(Al, W), especially the Ti, Ta, Hf, Nb, V and Zr.
2. The bulk moduli B^{VRH} and shear moduli G^{VRH} of the TM-substituted Co_3(Al, W) change as a function of volume changes and electron density. When TM occupying the Al sites, strong covalent bonding and symmetrical distribution of charge density can enhance the shear moduli. In the case of occupying the Co sites, the covalent strengthening effect is weakened by asymmetrical charge distribution, resulting in a decrease in shear moduli.
3. The addition of TM, especially Hf, Ti, Ta, Zr, Nb and Mo, would increase the relative phase stability of γ′-Co_3(Al, W) at high temperatures. In addition, the volume thermal expansion coefficients of γ′-Co_3(Al, W) after alloying Mn, Ir, Sc, Rh, Pt and Ni are very sensitive to temperature, and as a result, would not be good candidates for improving the structural stability of γ′-Co_3(Al, W).

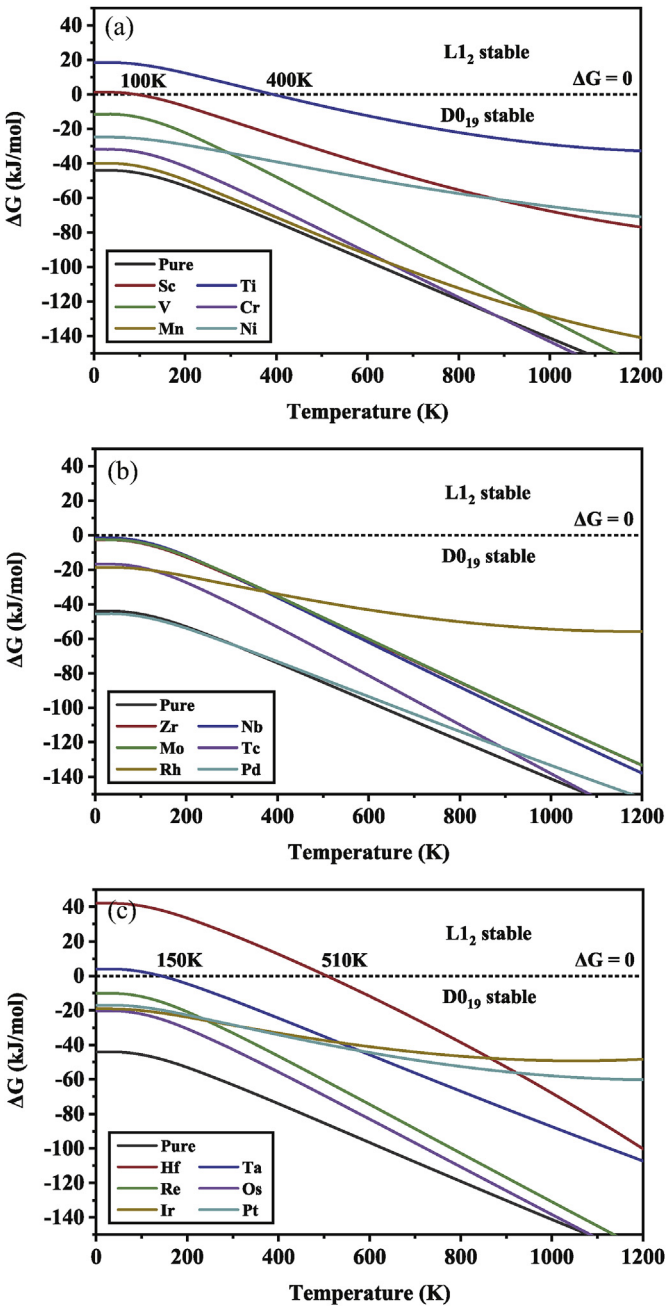

Fig. 7. The calculated ΔG of TM-substituted Co_3(Al, W); (a)3d TM elements; (b)4d TM elements; (c)5d TM elements.

Please cite this article as: X. Liu et al., Effects of transition elements on the site preference, elastic properties and phase stability of $L1_2$ γ′-Co_3(Al, W) from first-principles calculations, Journal of Alloys and Compounds, https://doi.org/10.1016/j.jallcom.2019.153179

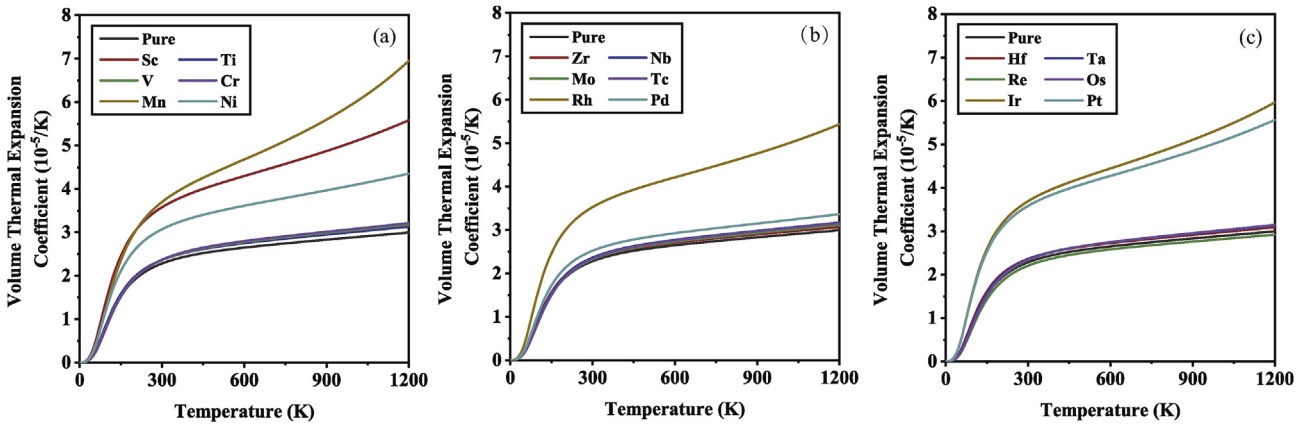

Fig. 8. The calculated volume thermal expansion coefficient α of TM-substituted Co_{ss}(Al, W); (a)3d TM elements; (b)4d TM elements; (c)5d TM elements.

Author contributions

1. Conceptualization, Xingjun Liu and Cuiping Wang.
2. Formal Analysis, Yichun Wang and Wei-Wei Xu.
3. Investigation, Yichun Wang and Wei-Wei Xu and Jiajia Han.
4. Original Draft Preparation, Yichun Wang and Wei-Wei Xu and Jiajia Han.
5. Writing-Review and Editing, Yichun Wang and Wei-Wei Xu and Jiajia Han.
6. Visualization, Yichun Wang and Wei-Wei Xu.
7. Supervision, Xingjun Liu and Cuiping Wang.

Declaration of competing interest

We declare that we have no financial and personal relationships with other people or organizations that can inappropriately influence our work, there is no professional or other personal interest of any nature or kind in any product, service and/or company that could be construed as influencing the position presented in, or the review of, the manuscript entitled.

Acknowledgements

This work was supported by the National Key Research and Development Program of China (Grant No. 2017YFB0702901), the National Natural Science Foundation of China (Grant Nos. 51831007, 51601161 and 51601160), and the Fundamental Research Funds for the Central Universities (Grant No. 20720170048).

Appendix A. Supplementary data

Supplementary data to this article can be found online at https://doi.org/10.1016/j.jallcom.2019.153179.

References

[1] J. Sato, T. Omori, K. Oikawa, I. Ohnuma, R. Kainuma, K. Ishida, Cobalt-base high-temperature alloys, Science 312 (2006) 90.
[2] M. Tsunekane, A. Suzuki, T.M. Pollock, Single-crystal solidification of new Co–Al–W-base alloys, Intermetallics 19 (2011) 636–643.
[3] T.M. Pollock, J. Dibbern, M. Tsunekane, J. Zhu, A. Suzuki, New Co-based γ-γ′ high-temperature alloys, J. Occup. Med. 62 (2010) 58–63.
[4] A. Bauer, S. Neumeier, F. Pyczak, R.F. Singer, M. Göken, Creep properties of different γ′-strengthened Co-base superalloys, Mater. Sci. Eng. A 550 (2012) 333–341.
[5] E.A. Lass, M.E. Williams, C.E. Campbell, K.-W. Moon, U.R. Kattner, Γ′ phase stability and phase equilibrium in ternary Co-Al-W at 900 °C, J. Phase Equilibria Diffusion 35 (2014) 711–723.
[6] A. Suzuki, High-temperature strength and deformation of γ/γ′ two-phase Co–Al–W-base alloys, Acta Mater. 56 (2008) 1288–1297.
[7] T. Omori, K. Oikawa, J. Sato, I. Ohnuma, U.R. Kattner, R. Kainuma, K. Ishida, Partition behavior of alloying elements and phase transformation temperatures in Co–Al–W-base quaternary systems, Intermetallics 32 (2013) 274–283.
[8] M. Ooshima, K. Tanaka, N.L. Okamoto, K. Kishida, H. Inui, Effects of quaternary alloying elements on the γ′ solvus temperature of Co–Al–W based alloys with fcc/L12 two-phase microstructures, J. Alloy. Comp. 508 (2010) 71–78.
[9] A. Bauer, S. Neumeier, F. Pyczak, M. Göken, Microstructure and creep strength of different γ/γ′-strengthened Co-base superalloy variants, Scr. Mater. 63 (2010) 1197–1200.
[10] H.Y. Yan, V.A. Vorontsov, D. Dye, Alloying effects in polycrystalline γ′ strengthened Co–Al–W base alloys, Intermetallics 48 (2014) 44–53.
[11] M. Chen, C.-Y. Wang, First-principles investigation of the site preference and alloying effect of Mo, Ta and platinum group metals in γ′-Co3(Al,W), Scr. Mater. 60 (2009) 659–662.
[12] M. Chen, C.-Y. Wang, First-principle investigation of 3d transition metal elements in γ′-Co3(Al,W), J. Appl. Phys. 107 (2010).
[13] S. Meher, H.Y. Yan, S. Nag, D. Dye, R. Banerjee, Solute partitioning and site preference in γ/γ′ cobalt-base alloys, Scr. Mater. 67 (2012) 850–853.
[14] S. Meher, R. Banerjee, Partitioning and site occupancy of Ta and Mo in Co-base γ/γ′ alloys studied by atom probe tomography, Intermetallics 49 (2014) 138–142.
[15] I. Povstugar, P.-P. Choi, S. Neumeier, A. Bauer, C.H. Zenk, M. Göken, D. Raabe, Elemental partitioning and mechanical properties of Ti- and Ta-containing Co–Al–W-base superalloys studied by atom probe tomography and nanoindentation, Acta Mater. 78 (2014) 78–85.
[16] C. Jiang, First-principles study of Co3(Al,W) alloys using special quasi-random structures, Scr. Mater. 59 (2008) 1075–1078.
[17] J.E. Saal, C. Wolverton, Thermodynamic stability of Co–Al–W L12 γ′, Acta Mater. 61 (2013) 2330–2338.
[18] W. Xu, Y. Wang, C. Wang, X. Liu, Z.-K. Liu, Alloying effects of Ta on the mechanical properties of γ′ Co3(Al, W): a first-principles study, Scr. Mater. 100 (2015) 5–8.
[19] C. Freysoldt, B. Grabowski, T. Hickel, J. Neugebauer, G. Kresse, A. Janotti, C.G. Van de Walle, First-principles calculations for point defects in solids, Rev. Mod. Phys. 86 (2014) 253–305.
[20] V. Stevanović, S. Lany, X. Zhang, A. Zunger, Correcting density functional theory for accurate predictions of compound enthalpies of formation: fitted elemental-phase reference energies, Phys. Rev. B 85 (2012), 115104.
[21] S. Shang, Y. Wang, Z.-K. Liu, First-principles elastic constants of α- and θ-Al2O3, Appl. Phys. Lett. 90 (2007).
[22] D.E. Kim, S.L. Shang, Z.K. Liu, Effects of alloying elements on elastic properties of Ni3Al by first-principles calculations, Intermetallics 18 (2010) 1163–1171.
[23] W.J.T.L. Voigt, A determination of the elastic constants for beta-quartz, Lehrb. Krist. 40 (1928) 2856–2860.
[24] A.J.Z.A.M.M. Reuss, Calculation of the flow limits of mixed crystals on the basis of the plasticity of monocrystals 9 (1929) 49–58.
[25] D.H. Chung, W.R. Buessem, The Voigt-Reuss-Hill approximation and elastic moduli of polycrystalline MgO, CaF2, β-ZnS, ZnSe, and CdTe, J. Appl. Phys. 38 (1967) 2535–2540.
[26] G. Kresse, D. Joubert, From ultrasoft pseudopotentials to the projector augmented-wave method, Phys. Rev. B 59 (1999) 1758–1775.
[27] G. Kresse, J. Furthmüller, Efficient iterative schemes for ab initio total-energy calculations using a plane-wave basis set, Phys. Rev. B 54 (1996) 11169–11186.
[28] G. Kresse, J. Furthmüller, Efficiency of ab-initio total energy calculations for metals and semiconductors using a plane-wave basis set, Comput. Mater. Sci. 6 (1996) 15–50.
[29] J.P. Perdew, K. Burke, M. Ernzerhof, Generalized gradient approximation made

simple, Phys. Rev. Lett. 77 (1996) 3865–3868.
[30] I. Povstugar, C.H. Zenk, R. Li, P.P. Choi, S. Neumeier, O. Dolotko, M. Hoelzel, M. Göken, D. Raabe, Elemental partitioning, lattice misfit and creep behaviour of Cr containingγ' strengthened Co base superalloys, Mater. Sci. Technol. 32 (2016) 220–225.
[31] L. Wang, M. Oehring, Y. Liu, U. Lorenz, F. Pyczak, Site occupancy of alloying elements in the L12 structure determined by channeling enhanced micro-analysis in γ/γ' Co-9Al-9W-2X alloys, Acta Mater. 162 (2019) 176–188.
[32] P. Pandey, S.K. Makineni, A. Samanta, A. Sharma, S.M. Das, B. Nithin, C. Srivastava, A.K. Singh, D. Raabe, B. Gault, K. Chattopadhyay, Elemental site occupancy in the L12 A3B ordered intermetallic phase in Co-based superalloys and its influence on the microstructure, Acta Mater. 163 (2019) 140–153.
[33] Y.-J. Wang, C.-Y. Wang, A comparison of the ideal strength between L12Co3(Al,W) and Ni3Al under tension and shear from first-principles calculations, Appl. Phys. Lett. 94 (2009).
[34] K. Tanaka, T. Ohashi, K. Kishida, H. Inui, Single-crystal elastic constants of Co3(Al,W) with the L12 structure, Appl. Phys. Lett. 91 (2007).
[35] M. Born, Thermodynamics of crystals and melting, J. Chem. Phys. 7 (1939) 591–603.
[36] A.R. Miedema, F.R.d. Boer, P.F.d. Chatel, Empirical description of the role of electronegativity in alloy formation, J. Phys. F Met. Phys. 3 (1973) 1558.
[37] Li, P. Wu, Correlation of bulk modulus and the constituent element properties of binary intermetallic compounds, Chem. Mater. 13 (2001) 4642–4648.
[38] J.H. Rose, H.B. Shore, Uniform electron gas for transition metals: input parameters, Phys. Rev. B 48 (1993) 18254–18256.
[39] S.F. Pugh, XCII. Relations between the elastic moduli and the plastic properties of polycrystalline pure metals, Lond. Edinb. Dub. Philos. Mag. J. Sci. 45 (1954) 823–843.
[40] D.G. Pettifor, Theoretical predictions of structure and related properties of intermetallics, Mater. Sci. Technol. 8 (1992) 345–349.
[41] S.I. Ranganathan, M. Ostoja-Starzewski, Universal elastic anisotropy index, Phys. Rev. Lett. 101 (2008), 055504.
[42] A. Suzuki, H. Inui, T.M. Pollock, L12-Strengthened cobalt-base superalloys, Annu. Rev. Mater. Res. 45 (2015) 345–368.
[43] M.A. Blanco, E. Francisco, V. Luaña, GIBBS: isothermal-isobaric thermodynamics of solids from energy curves using a quasi-harmonic Debye model, Comput. Phys. Commun. 158 (2004) 57–72.
[44] A. Otero-de-la-Roza, D. Abbasi-Pérez, V. Luaña, Gibbs2: a new version of the quasiharmonic model code. II. Models for solid-state thermodynamics, features and implementation, Comput. Phys. Commun. 182 (2011) 2232–2248.

Please cite this article as: X. Liu et al., Effects of transition elements on the site preference, elastic properties and phase stability of $L1_2$ γ′-Co_3(Al, W) from first-principles calculations, Journal of Alloys and Compounds, https://doi.org/10.1016/j.jallcom.2019.153179